

Generalized finite element method using proper orthogonal decomposition

W. Aquino^{1,*}, J. C. Brigham², C. J. Earls¹, and N. Sukumar³

¹ *School of Civil and Environmental Engineering, Cornell University, Ithaca, NY 14853, USA*

² *Department of Civil and Environmental Engineering, University of Pittsburgh, Pittsburgh, PA 15260, USA*

³ *Department of Civil and Environmental Engineering, University of California, Davis, CA 95616, USA*

SUMMARY

A methodology is presented for generating enrichment functions in generalized finite element methods (GFEM) using experimental and/or simulated data. The approach is based on the proper orthogonal decomposition (POD) technique, which is used to generate low-order representations of data that contain general information about the solution of partial differential equations. One of the main challenges in such enriched finite element methods is knowing how to choose, *a priori*, enrichment functions that capture the nature of the solution of the governing equations. Proper orthogonal decomposition produces low-order subspaces, that are optimal in some norm, for approximating a given data set. For most problems, since the solution error in Galerkin methods is bounded by the error in the best approximation, one expects that the optimal approximation properties of POD

*Correspondence to: 313 Hollister Hall, Cornell University, Ithaca, NY 14853, USA. E-mail: wa27@cornell.edu

Contract/grant sponsor: NIH-NIBIB; contract/grant number: Grant #EB2002167-17

can be exploited to construct efficient enrichment functions. We demonstrate the potential of this approach through three numerical examples. Best-approximation studies are conducted that reveal the advantages of using POD modes as enrichment functions in GFEM over a conventional POD basis.

Copyright © 2008 John Wiley & Sons, Ltd.

KEY WORDS: POD, partition of unity, enrichment, enriched finite elements, generalized finite element method

1. INTRODUCTION

The generalized finite element method (GFEM) [1] adopts the partition of unity approach as introduced by Melenk and Babuška [2, 3] to construct richer ansatz spaces for the solution of partial differential equations (PDEs). One advantage of the GFEM over the finite element method (FEM) is that it permits the use of compactly-supported non-polynomial bases in the solution process. However, in many instances, it is not apparent how to choose appropriate functions, or even type of functions, to produce effective approximations. As indicated by Babuška *et al.* [4], the central idea behind selecting efficient enrichment functions for GFEM is that the chosen function should reflect the nature of the solution to a given PDE or sets of PDEs. Babuška and co-workers go on to furnish an approach for selecting basis functions based on the knowledge about the function spaces where the solution to the PDE lives.

The GFEM allows for the use of very general functions, or mappings, as a basis for representing the solution. For crack modeling, Belytschko and Black [5] used the asymptotic crack-tip functions as enrichments within the partition of unity framework. However, enrichment functions need not be known solely in closed-form—results from numerical

simulations can also be used as demonstrated in the work of Strouboulis and co-workers [6, 7]. The latter authors used canonical domains containing features such as branched cracks, or closely spaced voids, to generate what they called mesh-based handbook functions. This approach is very useful for situations in which analytical expressions, which reflect the nature of the solution, are not available for enrichment. The contributions of Duarte *et al.* [8] on the application of global-local enrichment functions in three-dimensional fracture, and those of Sukumar and Pask [9] on the use of isolated atomic solutions as enrichment functions to solve the Schrödinger equation, are other instances where numerical simulations have been successfully used to construct enriched bases in generalized finite element methods.

One of the main difficulties that arise in using numerical solutions as enrichment functions in GFEM is the choice of essential and natural boundary conditions in the subproblems from which the enrichment functions are generated. Since boundary conditions play a fundamental role in the nature of the solution, careful selection of these is crucial for producing effective enrichments. Furthermore, material properties are also very important in the behavior of the solution to the boundary-value problem. Therefore, it is desirable to have a technique that can condense knowledge about the effects of various boundary conditions and material properties on the solution of a PDE into a low-dimensional basis. In turn, these basis functions could then be used as enrichment functions to solve boundary-value problems for different combinations of material properties and boundary conditions. The proper orthogonal decomposition (POD) technique [10] offers the possibility of generating such bases.

The main objective in POD is to obtain an optimal low-dimensional basis for representing an ensemble of high-dimensional experimental or simulated data [10]. This low-dimensional

basis can in turn be used to formulate reduced-order models of complex systems [11]. POD provides the means for condensing important information about the effect of a wide spectrum of material properties and boundary conditions on the nature of a PDE solution. Hence, it is conceivable to think that POD can be an effective technique for constructing efficient bases in GFEM. Furthermore, a POD-enriched basis can be used for constructing reduced-order models of problems whose domains differ from those of the modes. To the best knowledge of the authors, the latter is not possible using classical POD-based reduced order modeling techniques.

The remainder of this paper is organized as follows. First, a brief background is given on the theoretical foundations of GFEM and POD, which form the basis for the construction of modes as enrichment functions. In Section 3, the formulation of the POD-GFEM is given for a Helmholtz problem. Three numerical examples are presented to demonstrate the capabilities and potential of the proposed method, including a study on the L_2 -best approximation properties of the method (Section 4). Future directions and conclusions are presented in Section 5.

2. BACKGROUND

The essentials of the generalized finite element method and proper orthogonal decomposition are presented. The interested reader can refer to References [1, 4] and References [10, 11] for further details on GFEM and POD, respectively.

2.1. Generalized Finite Element Method

In this paper, we consider variational boundary-value problems that can be written in the following form: Find $u \in \mathcal{U}$ such that

$$b(u, w) = l(w) \quad \forall w \in H_0^1(\Omega), \quad (1a)$$

$$\mathcal{U} = \{u : u \in H^1(\Omega), u = \bar{u} \text{ on } \partial\Omega\}, \quad (1b)$$

where Ω is a bounded domain, u is the trial solution, w is the test function, $b(u, w)$ is a bilinear form, $l(w)$ is a linear functional, and \bar{u} is the prescribed Dirichlet (essential) boundary condition on $\partial\Omega$. In the above equation, the Sobolev space, $H^1(\Omega)$, consists of functions that are square-integrable in Ω up to first derivatives, and $H_0^1(\Omega)$ refers to the space that contains functions in $H^1(\Omega)$ that also vanish on the boundary $\partial\Omega$.

The discrete problem is obtained by introducing finite dimensional spaces $\mathcal{U}^h \subset \mathcal{U}$ and restating the above variational problem as: Find $u^h \in \mathcal{U}^h$ such that

$$b(u^h, w^h) = l(w^h) \quad \forall w^h \in H_0^1(\Omega). \quad (2)$$

In the generalized finite element method, trial solutions belong to a space that is a direct sum of the classical polynomial finite element space and a general function space. The members of the latter are compactly supported by virtue of employing a partition of unity approach. The trial solution (scalar-valued) is written as

$$u^h(\mathbf{x}) = \sum_{i \in I} N_i(\mathbf{x}) u_i + \sum_{\alpha} \sum_{j \in I} N_j(\mathbf{x}) \psi_{\alpha}(\mathbf{x}) a_{j\alpha}, \quad (3)$$

where I is the index set that consists of all nodes in the mesh, $N_i(\mathbf{x})$ is the FE basis function of node i , $\psi_{\alpha}(\mathbf{x})$ are enrichment functions, and u_i and $a_{j\alpha}$ are classical and enriched nodal

coefficients, respectively. In this study, the test functions are approximated using the same basis functions as those used for the trial solution.

2.2. A Priori Error Estimate

Melenk and Babuška [2] showed the following *a priori* error estimate, which forms the backbone of the analysis of the generalized finite element method. First, we know that the set $\{N_i(\mathbf{x})\}$ forms a partition of unity. Let Ω_i be the support of $N_i(\mathbf{x})$ and define locally on each patch a function

$$f_i(\mathbf{x}) = \sum_{\alpha} a_{i\alpha} \psi_{\alpha}(\mathbf{x}). \quad (4)$$

If

$$\|u - f_i\|_{L_2(\Omega_i)} \leq \epsilon(i), \quad \epsilon(i) > 0, \quad (5)$$

then, defining

$$u^{PU}(\mathbf{x}) = \sum_{\alpha} \sum_i N_i(\mathbf{x}) f_i(\mathbf{x}),$$

the approximation error is bounded as

$$\|u - u^{PU}\|_{L_2(\Omega)} \leq C_1 \left[\sum_i \epsilon(i)^2 \right]^{\frac{1}{2}}. \quad (6)$$

In the above equation, u is the solution being approximated, C_1 is a constant independent of ϵ , but which may depend on the element size, h , and the quality of the mesh (i.e. element distortion).

This error estimate is a powerful result. It indicates that, in the partition of unity finite element method (PUFEM), the rate of convergence of the global solution is governed by the local approximation properties of the enrichment functions. To estimate the error in GFEM,

notice that the approximation lives in the union of the polynomial finite element space and a general function space. For the finite element part of the approximation, the error is bounded as

$$\|u - u^{FEM}\|_{L_2(\Omega)} \leq C_2 h^{p+1} \|u\|_{p+1}. \quad (7)$$

Where C_2 is a constant that may depend on the element size [12], and p is the order of the polynomial. Then, it is not difficult to show that the error in GFEM is bounded by the minimum of the errors shown in Eq. (6) and Eq. (7).

2.3. Proper Orthogonal Decomposition

For simplicity, the derivations presented herein consider scalar fields only. However, the extension to vector fields is straightforward and can be found in Reference [10]. The following derivations are carried out in the Hilbert space L_2 defined as

$$L_2 = \left\{ f(\mathbf{x}) : \int_{\Omega} f^2 d\Omega < \infty, \mathbf{x} \in \Omega \subset \mathbb{R}^3 \right\} \quad (8a)$$

with inner product

$$(f, g) = \int_{\Omega} fg d\Omega \quad \forall f, g \in L_2 \quad (8b)$$

and norm

$$\|f\| = (f, f)^{\frac{1}{2}}. \quad (8c)$$

Consider an ensemble of functions $\{f_k(\mathbf{x})\}_{k=1}^n \in L_2$. The main goal in POD is to find a sequence of subspaces such that the average distance between the members of the ensemble and these subspaces is minimal, i.e., finite-dimensional representations of the form

$$f(\mathbf{x}) \approx \sum_{i=1}^m a_i \phi_i(\mathbf{x})$$

are sought such that members of the data ensemble are approximated, in some optimal sense, by the above expansion.

Consider a finite-dimensional space $V^m = \text{span}\{\phi_i\}_{i=1}^m$, $V^m \subset L_2$. The best approximation in V^m to a given function f_k of the ensemble is defined as

$$\|f_k - f_k^*\| \leq \|f_k - v\| \quad \forall v \in V^m,$$

where f_k^* is the best approximation in V^m . For an orthogonal basis, the best approximation can be computed as [13]

$$f_k^* = \sum_{i=1}^m \frac{(f_k, \phi_i)}{\|\phi_i\|^2} \phi_i.$$

A suitable basis can be constructed by finding the subspace V_m whose best approximation is closest to the ensemble of functions $\{f_k(\mathbf{x})\}_{k=1}^n$ in an average sense. This is accomplished by solving the following optimization problem:

$$\min_{\phi_i \in L_2} \left\langle \|f_k - f_k^*\|^2 \right\rangle \quad \ni \|\phi_i\| = 1 \quad (i = 1, \dots, m).$$

The averaging operation is defined as

$$\langle f_k \rangle = \frac{1}{m} \sum_{k=1}^m f_k.$$

It can be shown (see Reference [11]) that the above minimization problem is equivalent to the following maximization problem:

$$\max_{\phi_i \in L_2} \left\langle (f_k, \phi_i)^2 \right\rangle \quad \ni \|\phi_i\| = 1 \quad (i = 1, \dots, m).$$

Defining the functional

$$J(\phi_i) = \left\langle (f_k, \phi_i)^2 \right\rangle - \lambda \left(\|\phi_i\|^2 - 1 \right),$$

where the variable λ is a Lagrange multiplier that enforces the constraint of unit norm on the basis functions, the maximization problem is solved by setting the Gateaux derivative of the functional to zero and solving the resulting eigenvalue problem, i.e.,

$$\left. \frac{d}{d\varepsilon} J(\phi_i + \varepsilon\eta) \right|_{\varepsilon=0} = 0 \quad \forall \eta \in L_2.$$

The eigenvalue problem resulting from the above operation is

$$\int_{\Omega} \langle f_k(\mathbf{x}) f_k(\xi) \rangle \phi_i(\mathbf{x}) d\mathbf{x} = \lambda \phi_i(\xi). \quad (9)$$

Direct discretization of the above equation leads, in general, to a very large and computationally demanding eigenvalue problem. Therefore, the method of snapshots is commonly used to transform the above eigenvalue problem into a much smaller and tractable one. A detailed formulation of the method of snapshots can be found in References [11,14,15]. For completeness, the main equations are provided herein. In the method of snapshots, the eigenvalue problem defined in Eq. (9) is transformed into the following eigenvalue problem:

$$\frac{1}{m} \sum_{k=1}^m A_{jk} C_k = \lambda_j C_j, \quad (10a)$$

$$A_{jk} = \int_{\Omega} f_j(\xi) f_k(\xi) d\xi. \quad (10b)$$

Once the eigenvalue problem in Eq. (10) is solved, the r th proper orthogonal mode is computed as

$$\phi_r(\mathbf{x}) = \frac{1}{\lambda^r m} \sum_{k=1}^m f_k(\mathbf{x}) C_k^r.$$

The proper orthogonal modes obtained through the method of snapshots shown above are orthogonal, but not orthonormal. To achieve orthonormality, we can define normalized

eigenvectors as

$$\{C^{*r}\} = \frac{\sqrt{m\lambda^r}}{\sqrt{\sum_{i=1}^m C_i^r C_i^r}} \{C^r\}.$$

The above eigenvectors are used in place of $\{C\}$ in Eq. (10). It can be easily shown that on using this substitution, the proper orthogonal modes are now orthonormal, i.e., $(\phi_i, \phi_j) = \delta_{ij}$, where δ_{ij} is the Kronecker-delta.

3. FORMULATION AND IMPLEMENTATION

Due to their appealing approximation properties, proper orthogonal modes appear to be natural candidates to be used as enrichment functions in the generalized finite element method. These modes offer the possibility of incorporating features of the solution to a boundary-value problem by using numerical simulations and/or experimental data. For a POD-GFEM formulation, the POD modes $\phi_\alpha(\mathbf{x})$ are used as the enrichment functions $\psi_\alpha(\mathbf{x})$ in Eq. (3). The domain of the modes can be, in general, different from the domain of the problem. This is a significant point of departure from the common use of POD in the construction of reduced-order models [11].

We now show important details of the GFEM and the incorporation of POD modes as function approximations. For the numerical examples presented in the next section, we use a model problem from acoustics based on the Helmholtz equation. The strong form of the boundary-value problem is:

$$\nabla^2 u + k^2 u + g = 0 \text{ in } \Omega \subset \mathbb{R}^2, \quad u = \bar{u} \text{ on } \Gamma = \partial\Omega, \quad (11)$$

where k is the wave number, u is the acoustic pressure, and g is a forcing function. Without

loss of generality, we assume that constant Dirichlet boundary conditions are applied over the entire boundary Γ . The associated variational statement of Eq. (11) is of the form given in Eq. (1) with

$$b(u, w) = \int_{\Omega} \nabla u \cdot \nabla w \, d\Omega - k^2 \int_{\Omega} uw \, d\Omega, \quad (12a)$$

$$l(w) = \int_{\Omega} gw \, d\Omega. \quad (12b)$$

For simplicity and clarity, we will work with basis functions defined globally (i.e., over the domain Ω) as opposed to shape functions defined over an elemental domain. The usual assembly operations in finite element methods are tacit in the formulation.

The GFEM basis function vector is the union of the classical finite element polynomial bases, $\{N_i\}_{i=1}^s$, and the enriched bases, $\{N_i\phi_p\}_{i=1}^s$ ($p = 1, 2, \dots, m$). The number of nodes in the mesh is s and m is the number of enrichment functions (POD modes). Define a row vector of length $(m + 1)s$ that contains the generalized finite element basis:

$$[N_g] = [N_1 \ N_2 \ \dots \ N_s \ N_1\phi_1 \ N_2\phi_1 \ \dots \ N_s\phi_1 \ \dots \ N_1\phi_m \ N_2\phi_m \ \dots \ N_s\phi_m]. \quad (13)$$

The nodal coefficients that correspond to the generalized finite element basis functions are defined in a column vector $\{d\}$:

$$\{d\} = \{u_1 \ u_2 \ \dots \ u_s \ a_{11} \ a_{21} \ \dots \ a_{s1} \ \dots \ a_{1m} \ a_{2m} \ \dots \ a_{sm}\}^T. \quad (14)$$

Using Eqs. (3), (13) and (14), we can express the trial function and its gradient as

$$u^h = [N_g]\{d\}, \quad \nabla u^h = [B_g]\{d\}, \quad (15a)$$

$$[B_g] = \begin{bmatrix} N_{1,1} & N_{2,1} & \dots & N_{s,1} & \dots & (N_1\phi_m)_{,1} & (N_2\phi_m)_{,1} & \dots & (N_s\phi_m)_{,1} \\ N_{1,2} & N_{2,2} & \dots & N_{s,2} & \dots & (N_1\phi_m)_{,2} & (N_2\phi_m)_{,2} & \dots & (N_s\phi_m)_{,2} \end{bmatrix}, \quad (15b)$$

where $(\cdot)_{,i}$ denotes the partial derivative of the argument with respect to the i th coordinate-direction.

Substituting the trial and test approximation of the form given in the above equation into Eq. (2), and on using the arbitrariness of nodal variations, the following discrete system of equations is obtained:

$$[K]\{d\} = \{p\}, \quad (16a)$$

$$[K] = \int_{\Omega} [B_g]^T [B_g] d\Omega - k^2 \int_{\Omega} [N_g]^T [N_g] d\Omega, \quad \{p\} = \int_{\Omega} [N_g]^T g d\Omega. \quad (16b)$$

We point out that the solution of Helmholtz equation via partition of unity methods has been investigated by many researchers; the interested reader can refer to Strouboulis *et al.* [16], and the references therein, for details. For the problem under consideration, it is important to recognize that essential boundary conditions can be handled in a straightforward manner in the above formulation. A simple strategy is to treat essential boundary conditions as is commonly handled in the finite element method—the nodal coefficients of the finite element basis are set to the prescribed value whereas those of the enriched basis are set to zero on the essential boundary. Although simple, this approach may not be accurate for coarse meshes and spatially-varying boundary conditions. A more accurate approach would be to compute the best approximation to the essential boundary conditions using the entire basis through a least squares approach.

We now provide details on the numerical treatment of the POD modes in the implementation of the method. The modes are interpolated using finite element basis functions as

$$\phi_{\alpha}^h(\mathbf{x}) = \sum_i N_i(\mathbf{x}) \phi_{i\alpha}, \quad (17)$$

where $\{\phi_\alpha\}$ is a column vector that contains the nodal values of mode α . The finite element mesh used for generating the snapshots was also used for approximating the modes, but the mesh used for the POD-GFEM was, in general, distinct. We used a Galerkin projection approach to smooth the derivatives of the modes before using them in Eq. (15). Details of this smoothing approach can be found in Reference [17].

3.1. Data Generation for Constructing the POD Modes

The information in the modes regarding the solution to a PDE depends entirely on the data set (i.e., snapshots) from which the modes are constructed. Hence, it is of paramount importance that the data be selected judiciously. One way to look at this problem is from the statistical learning viewpoint, i.e., the POD modes are “trained” on the information carried by the data. Therefore, many of the approaches used in the machine and statistical learning literature could be useful for generating data from which to build the POD modes.

It is important to use *a priori* knowledge about the problem at hand in producing the snapshots. For instance, if the type and character of the boundary conditions of the problem are known, it would be of great advantage to generate the snapshots using these conditions. This simple concept also applies to other aspects of the problem such as geometric features, material structure, etc. At the same time, it is important to bear in mind that the computational cost for generating the data (if simulated data is used) should be kept low. Otherwise, the appeal of the method quickly vanishes.

In the absence of specific information about boundary conditions, material models, etc., a maximum entropy approach can be used to generate the snapshots [18]. For instance, assume

that we need to produce a set of snapshots to build a POD basis that would be suitable for a range of wave numbers in the Helmholtz problem given in Eq. (11). To this end, we can sample q wave speeds from a uniform distribution within some physically meaningful bounds. This approach can also be used for boundary conditions.

Thus far, we have discussed approaches for using data generated using numerical simulations. However, an advantage of proper orthogonal decomposition is that experimental, or field measurements, could be incorporated into the modes. For instance, digital particle image velocimetry (PIV) has been used by Ma *et al.* [19] to produce POD modes that were used in Galerkin-based reduced-order models of the Navier-Stokes equations in fluid dynamics. The same modes could be used in the generalized finite element method proposed herein. An advantage of our proposed method over the conventional model reduction approach would be that in GFEM the POD modes can be used on domains that are distinct from the ones on which the data was generated due to the local character of the partition of unity approach.

4. NUMERICAL RESULTS

In this section, the performance of the POD-GFEM is demonstrated through three numerical examples. The first two examples are based on the Helmholtz problem described in Section 3. The third problem demonstrates the performance of the method in a nonlinear heat transfer problem with a heat source that moves along a quasi-compactly-supported path. These examples were selected since they have features that best highlight the advantages and potential of the POD-GFEM. We now define important notation that will be used in the numerical examples that follow. The domain and boundary of the problem to be solved will

be denoted by Ω and Γ , respectively, whereas Ω_{POD} and Γ_{POD} , respectively, will be used for the domain and boundary on which the POD modes are defined.

An important aspect in generalized finite element methods is numerical integration. It is well-known that due to the presence of non-polynomial enriched bases, generalized finite element methods require higher-order numerical integration rules. All problems that follow were solved with increasing tensor-product Gauss quadrature rules until the solution did not change beyond a predefined tolerance. This step was carried out to ensure that the error in the solution due to numerical integration was insignificant in comparison to the approximation error. For instance, in Examples 1 and 2, a 20×20 quadrature rule was necessary, whereas for four modes an 80×80 rule was needed. For Example 3, a 30×30 quadrature rule was sufficient when four modes were used as enrichment functions. Furthermore, a direct sparse solver was used for the linear systems in all the numerical simulations presented herein.

4.1. Example 1: Helmholtz Problem with Coincident Domains

In this problem, the domain for the modes and the domain of the problem are chosen to be the same (i.e., $\Omega = \Omega_{\text{POD}}, \Gamma = \Gamma_{\text{POD}}$). It is important to point out that this is the common approach followed when proper orthogonal decomposition is used in the context of reduced-order modeling. However, as we will show in this section, the POD-GFEM offers unique capabilities not present in conventional reduced-order modeling approaches.

The domain and boundary conditions for this first example are shown in the left sketch in Figure 1. In addition, the reference solution of this example problem is shown in the right plot in Figure 1. The bulk modulus, B , and density, ρ , of the medium were taken as 2200 GPa and

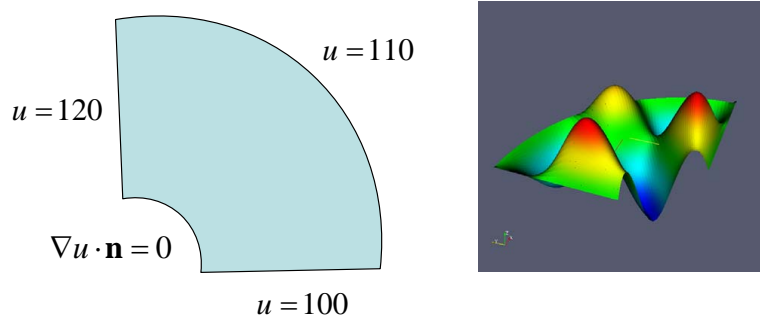


Figure 1. Domain and boundary conditions for Examples 1 and 2 (left). Reference solution for Example 1 (right).

1000 kg/m³, respectively. It is important to bear in mind that the wave number k is given in terms of the bulk modulus, density and circular frequency as

$$k^2 = \omega^2 \frac{B}{\rho}.$$

Two frequency ranges were used for the problem. These frequency ranges were 2000–3500 Hz and 3500–4500 Hz. These frequency ranges were selected so that they yielded low wave numbers to avoid issues related to the well-known pollution effect that arises from the Helmholtz equation [20].

The snapshots for the construction of the POD modes were generated from FE simulations that used a very fine mesh (10,000 biquadratic elements). A total of ninety six snapshots were used and were sampled as follows. First, they were evenly spaced in increments of 100 Hz in the frequency range 2000–3500 Hz. Then, six different combinations of boundary conditions were considered. Three of these combinations included Dirichlet boundary conditions on all sides and the other three included different values of Neumann boundary conditions on all sides. The values for the Dirichlet boundary conditions were randomly selected in the range

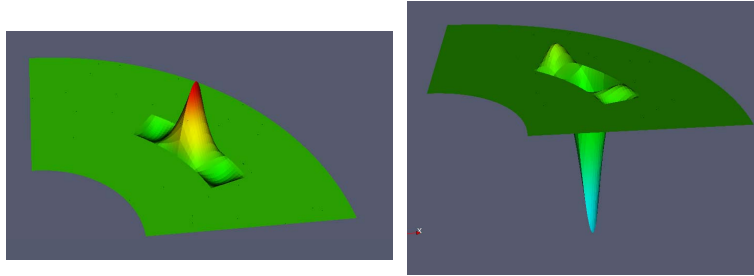


Figure 2. The left plot shows one of the FEM polynomial basis functions (i.e. partition of unity), while the right picture shows the enriched basis function (using the first POD mode as enrichment).

100–500, whereas the Neumann boundary conditions were randomly selected from the range 1–4. Notice that these arrangements of boundary conditions do not include the case depicted in the left sketch of Figure 1. In the language of statistical learning, we state that the test case was not considered in the training data, i.e., the selected case for boundary conditions will test the extrapolation capabilities of the method. Moreover, these extrapolation capabilities will be further tested by solving the problem in the frequency range 3500–4500 Hz, which is different from the one used for generating the snapshots. Figure 2 shows a polynomial basis function for a biquadratic mapped element (left plot) and an enriched basis function (i.e. product of this shape function and the first POD mode) for Example 1 (right plot).

The domain shown in Figure 1 was divided into 25 biquadratic (i.e., 9 nodes) finite elements. This is indeed a coarse mesh for this problem. For the POD-GFEM, a coarse mesh with 25 biquadratic finite elements was used, and then enriched progressively with 1, 2, 3, and 4 modes. For the results presented for FEM, biquadratic elements were used, but with progressively finer meshes. To study the performance of the method, we computed the relative L_2 error

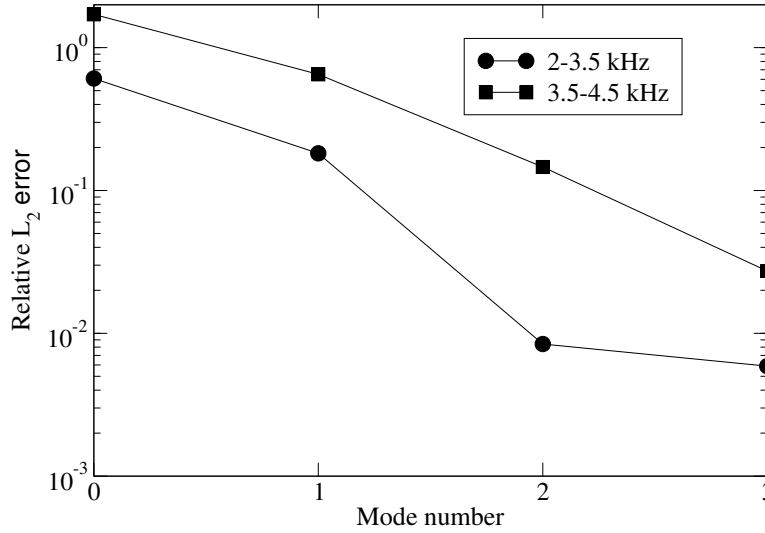


Figure 3. Relative L_2 error versus number of modes for two different frequency ranges.

between the GFEM solution and the solution obtained with the finite element mesh (i.e. 10,000 biquadratic elements), which will be regarded as the reference solution. Figure 3 shows the relative L_2 error versus number of POD modes for the two frequency ranges considered in the problem. The case for zero modes corresponds to the coarse finite element mesh without enrichment. The relative error used in this paper is defined as

$$e = \frac{\|u - u^h\|}{\|u\|}.$$

As illustrated in Figure 3, and consistent with expectations, the error decreases with increasing number of modes. There was a decrease of over an order of magnitude when three modes were used as compared to the case when the coarse mesh was used without enrichment. Although the results were less accurate for the frequency range 3500–4500 Hz than for the previous range, a significant improvement (nearly two orders of magnitude) in the error was still observed when

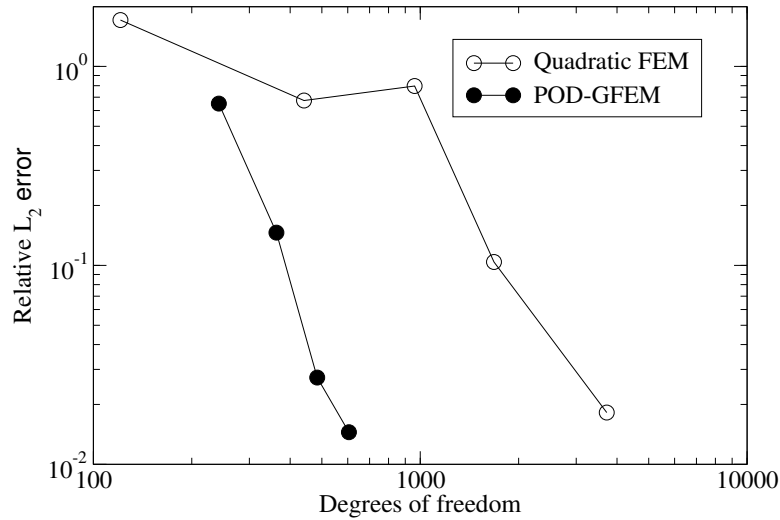


Figure 4. Relative L_2 error versus degrees of freedom for FEM and POD-GFEM. Frequency range: 3500–4500 Hz.

POD modes were used for enrichment. These results point to the robustness of the POD-GFEM as it can extrapolate to cases not included in the generation of the snapshots. It is interesting to observe that the use of very few modes alone is sufficient to result in drastic reduction in the error. The relative L_2 error obtained for FEM and POD-GFEM are presented in Figure 4. The plot in Figure 4 demonstrates that for the same error, the POD-GFEM requires far fewer degrees of freedom than the conventional FEM. We would like to point out that the non-monotonic convergence displayed by the solution obtained with FEM is typical of Helmholtz equations with coarse meshes. This is due to the indefiniteness of the variational form. More details on this issue can be found in Reference [21].

The approximation capabilities of the POD modes in the context of GFEM were studied in order to understand the benefits of combining POD modes with polynomial spaces through a

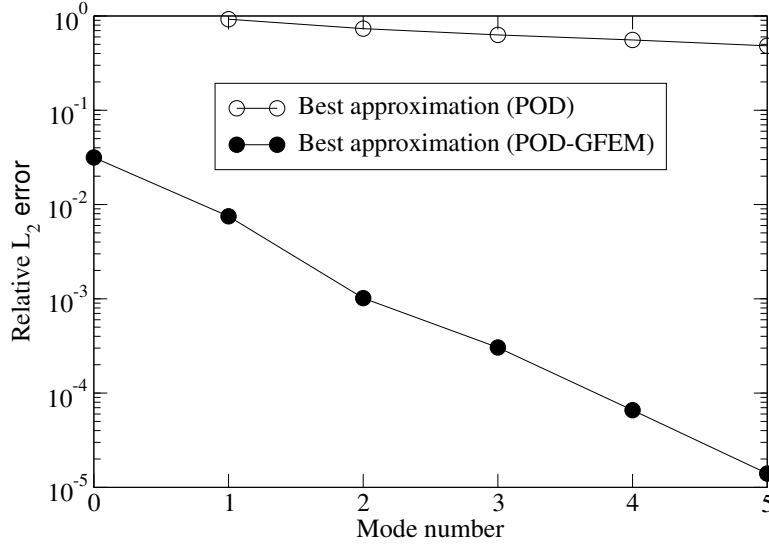


Figure 5. Best approximation relative L_2 error versus number of POD modes.

partition of unity approach. For this purpose, best approximations for POD and POD-GFEM bases were computed as follows. The best approximation in terms of POD modes and for the POD-GFEM were computed as

$$e_{\text{POD}} = \inf \frac{\left\| u - \sum_{i=1}^m a_i \phi_i \right\|}{\|u\|}, \quad (18a)$$

$$e_{\text{POD-GFEM}} = \inf \frac{\|u - u^h\|}{\|u\|}, \quad (18b)$$

where u^h is given in Eq. (15a). In the above equations, the field u represents the reference solution used in Example 1. The POD-GFEM approximation was built using the same FE mesh as was used in Example 1 (i.e. 25 biquadratic elements).

Figure 5 shows a plot of the relative L_2 -Error in best approximation for POD and POD-GFEM bases. Two important pieces of information can be extracted from this plot. First, notice

that, in the case of a pure POD basis, the first five modes are not sufficient for approximating the reference solution as revealed by the large relative error. Second, a strong contribution from the POD modes in the POD-GFEM basis is evident. Notice that there is a decrease of approximately an order of magnitude in relative error when only one mode is used in the POD-GFEM basis as compared to the coarse FE mesh (i.e., zero modes). In addition, this trend continues as additional modes are added. This improved approximation capability when POD modes are used in a GFEM context can be attributed to the compact support of the enriched basis. Compact support helps in capturing localized features of the solution that the global modes cannot accurately approximate.

These best approximation results are very significant for the method presented in this work since it is well known that the solution to the variational problem under consideration is bounded by the best approximation error (provided that the pollution error is negligible) [3].

4.2. Example 2: Helmholtz Problem with Non-Coincident Domains

A significant advantage of using POD modes in the context of the generalized finite element method is that the domain of the modes need not coincide with the domain of the problem under consideration [6, 7]. We illustrate this point through a numerical example in which the POD modes were obtained on a domain different from the problem domain. The problem and modes domains are shown in Figure 6. The problem for this example is the same as the one shown in Example 1. However, the modes domain was selected such that $\Omega \subset \Omega_{\text{POD}}$. For this example, the frequency range used for both, generating the snapshots, and for solving the problem, was 3500–4500 Hz. The snapshots were generated using the same approach that was

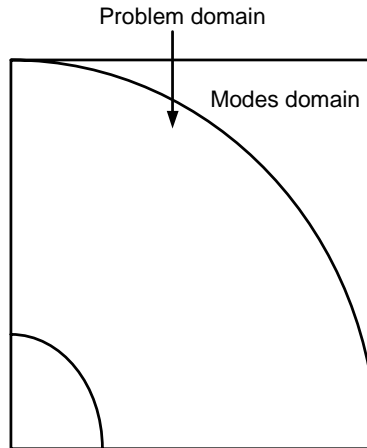


Figure 6. POD modes and problem domains used in Example 2.

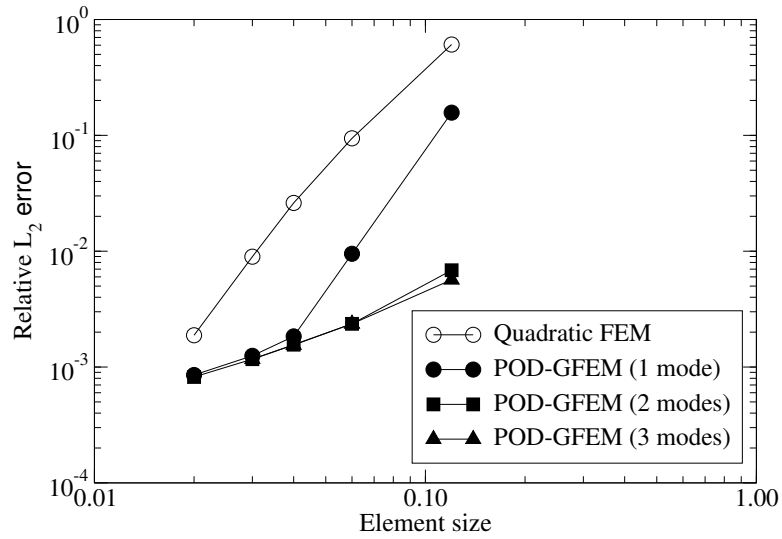


Figure 7. Relative error versus element size for Example 2.

described for Example 1.

Figure 7 shows a plot of the relative L_2 error versus element size. This plot illustrates the

results of an h -convergence study. The relative error was computed using progressively finer meshes and fixing the number of modes. It can be observed from Figure 7 that the relative error for coarse meshes in the POD-GFEM is significantly smaller than that of an equivalent mesh in FEM. In addition, as expected, the difference in the error for the FEM and the POD-GFEM is less pronounced as the mesh is refined. The reason for this is that as the element size decreases the polynomial and POD bases become locally similar.

Furthermore, it can be noticed that the improvement of the error upon h -refinement decreases as more POD modes are added. From the error estimate shown in Eq. (6), it is known that the global error in GFEM is governed by the local approximation capabilities of the enrichment functions. The results shown in Figure 7 indicate that the local error between the solution and the POD expansion reaches a plateau after a certain number of modes. This result was expected since the POD and problem domains were different. Hence, it would be very difficult for a POD expansion, regardless of its dimension, to approximate the solution arbitrarily close (locally). It is not surprising that the rate of convergence upon h refinement is different for FE and the proposed method. Notice that this rate of convergence is related to how the constant C_1 and each $\epsilon(i)$ in Eq. (6) depend on h , which is not trivially determined. A more detailed error analysis is needed to establish convergence rates for the method proposed herein. This is out of the scope of this paper and will be pursued by the authors in a sequel.

A plot of the relative L_2 -Error versus number of degrees of freedom (DOFs) is shown in Figure 8. As opposed to the h -convergence plot in Figure 7, this plot provides some information about the computational cost/benefit of adding modes to the POD-GFEM basis. It can be observed in Figure 8 that for relative errors around one percent far fewer DOFs are

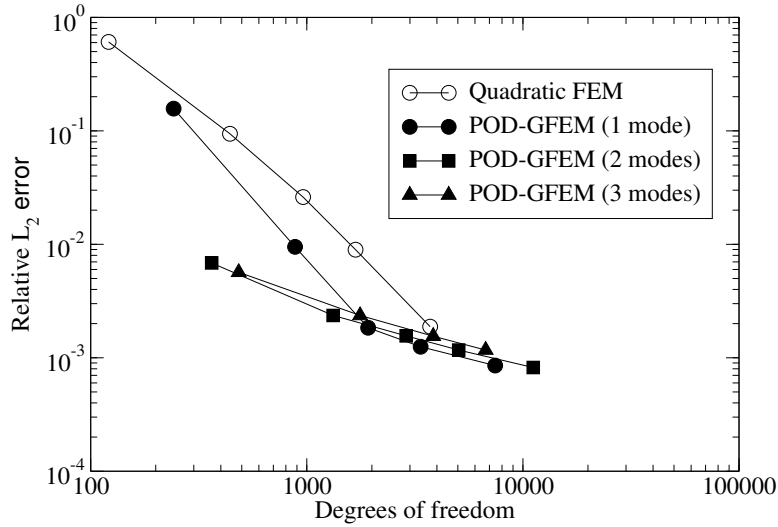


Figure 8. Relative error versus number of DOFs for Example 2.

needed in the POD-GFEM with two and three modes than for the FEM. However, the benefit of enriching with POD modes, in this problem, is less obvious for higher mesh densities. It is important to bear in mind that the latter is not a general result. How many modes are needed for a given accuracy depends on how well the modes capture the nature of the solution, which in turn depends on how the snapshots are generated as was discussed in Section 3.

Some remarks about the computational cost/benefit of the method are in order. Although the number of degrees of freedom may be significantly lower for POD-GFEM for relative errors around one percent, the implications on the relative computational cost between FEM and POD-GFEM should be interpreted carefully. It is important to bear in mind that the coefficient matrix is less sparse for the POD-GFEM than for the FEM, and that numerical integration is significantly more expensive for the POD-GFEM than for the FEM. Nonetheless, the authors

found that there are substantial benefits in terms of lower computer memory use and faster solution of the system of equations in POD-GFEM. Moreover, the reader should bear in mind that generating POD modes can be computationally expensive as well, but this task needs to be performed only once and these modes could be used for different problems.

4.3. Example 3: Nonlinear Heat Transfer

The third example is a nonlinear heat transfer problem. This problem consists of a moving localized heat source (e.g., simulating welding) in a square domain. This problem was designed to further show the advantage of using the POD-GFEM formulation, as compared to a conventional POD reduced order modeling approach. Because of the localized nature of the solution (i.e., localized heat source), it is evident that it would be difficult to obtain, in general, satisfactory approximations to this problem using a conventional reduced-order modeling approach.

The initial-boundary value problem is posed as

$$\frac{\partial T}{\partial t} = \nabla \cdot (\alpha(T)\nabla T) + q(\mathbf{x}, t) \quad \text{in } \Omega, \quad (19a)$$

$$T(\mathbf{x}, t) = 25^\circ\text{C} \quad \text{on } \partial\Omega, \quad (19b)$$

$$T(\mathbf{x}, 0) = 25^\circ\text{C} \quad \text{in } \Omega, \quad (19c)$$

where T is temperature, t is time, q is the heat source, α is the thermal diffusivity, which is taken to be a function of temperature and given as

$$\alpha(T) = \frac{\kappa(T)}{\rho c},$$

where ρ is the density and c is the specific heat. The thermal conductivity as a function of

temperature is

$$\kappa(T) = 5 \times 10^{-8}T^3 - 9 \times 10^{-5}T^2 + 5.1 \times 10^{-3}T + 4.6 \times 10^4,$$

which is a slightly modified version of that given in Reference [22]. The localized heat source is described via the relation

$$q(\mathbf{x}, t) = \frac{Q}{\rho c} \exp\left(-\sum_{i=1}^d \frac{(x_i - v_i t - y_i)^2}{2E_i^2}\right),$$

where Q is the intensity of the source, \mathbf{x} is the current position of the source, \mathbf{y} is the initial position of the source, \mathbf{v} is the velocity, and E_i describes the extent of the source in the direction x_i . On integrating Eq. (19) in time, using the backward Euler algorithm, the variational form of the problem is given as: Find $T^k \in \mathcal{U}$ such that

$$b^k(T^k, w) = l^k(w) \quad \forall w \in H_0^1(\Omega), \quad (20a)$$

$$b^k(T^k, w) = \int_{\Omega} (\Delta t \alpha(T^k) \nabla w \cdot \nabla T^k + T^k w) d\Omega, \quad (20b)$$

$$l^k(w) = \int_{\Omega} w(T^{k-1} + \Delta t q^k) d\Omega. \quad (20c)$$

In the above equations, Δt is the time increment used for time integration, and the superscript k denotes a quantity evaluated at time t^k . The snapshots were generated from three simulations with the localized heat source moving along three different paths. The paths for each simulation are shown in Figure 9. For each simulation, the total time was three seconds using time intervals of 0.025 second; for a total of 120 time steps. The heat source moved with a fixed velocity of 1 m/sec for a time of one second, and then it was turned off for a cooling period of two seconds. The values for other material constants and model parameters used in this problem are shown in Table I. Forty equally spaced snapshots were selected from each simulation for

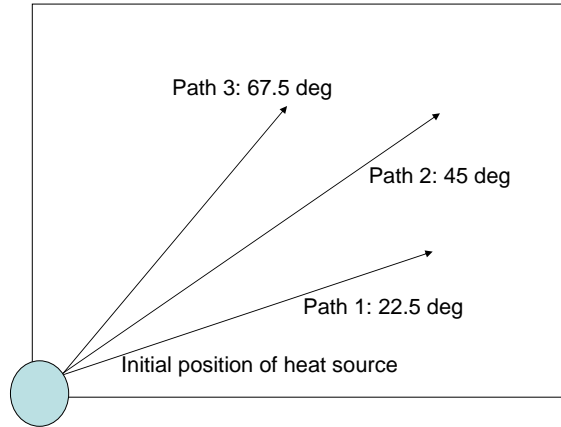


Figure 9. Domain and paths for the moving heat source used for generating the snapshots in Example

3. The dimensions are 1 m x 1 m.

Table I. Material constants and parameters used in Example 3.

Constant	Value
ρ	7850 kg/m ³
c	419 /kg-°C
Q	168548 W/m ³
E_1	0.025 m
E_2	0.025 m
v	1 m/s along path

a total of 120 snapshots from which the POD modes were computed. The first four POD modes are shown in Figure 10 in order of decreasing eigenvalues starting on the top left and moving clockwise. Notice the global character of the most influencing mode (Mode 1). This global character reflects the averaging nature of the proper orthogonal decomposition, making it difficult for a POD expansion with these first four modes to approximate the solution of the

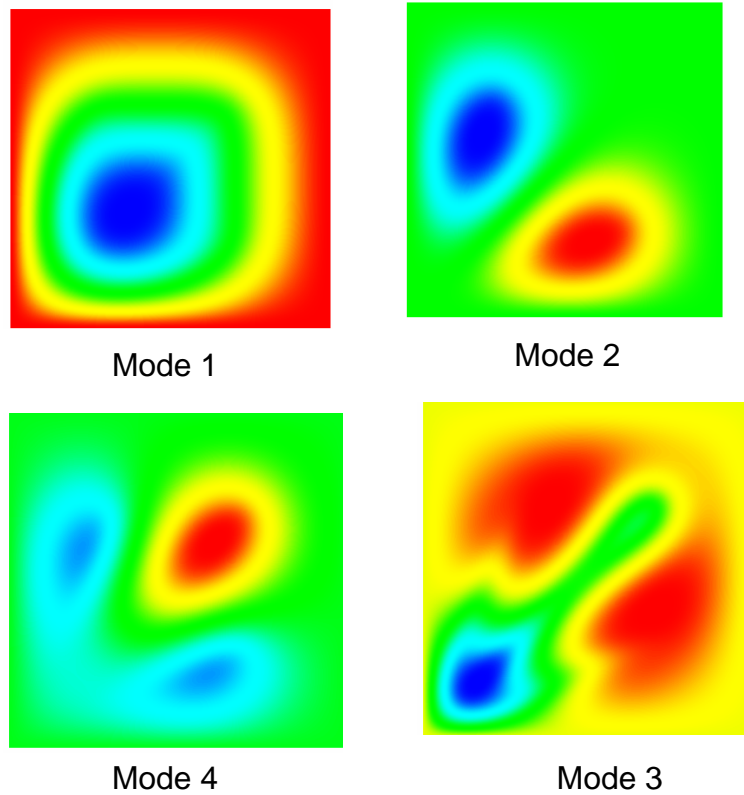


Figure 10. The four POD modes with largest eigenvalues in Example 3. The modes are arranged in descending order of eigenvalues.

present problem.

A generalized finite element basis using the first four modes as enrichment is used in the POD-GFEM to find an approximate solution. The path of the moving source was 45° and all the parameters used in generating the snapshots remained the same. Bilinear quadrilateral finite elements were used for this example. In order to compute approximation errors, a very fine mesh (300×300) was used to generate what was taken as the reference solution. Figure 11 shows three plots corresponding to the reference solution, the solution obtained

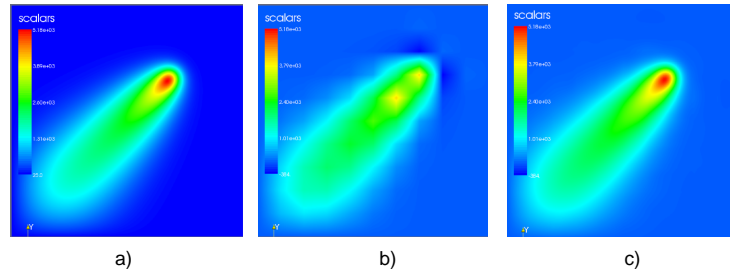


Figure 11. Temperature distribution at 1 second. (a) Reference solution; (b) FE solution corresponding to a coarse mesh (10×10); and (c) GFEM solution on a 10×10 mesh.

with a coarse (10×10) finite element mesh, and the solution obtained using the same coarse mesh, but enriched with four modes. It can be observed that, using the “eye norm”, the POD-GFEM produced a more accurate solution than that obtained using a coarse FE mesh. To quantify the benefit of POD-GFEM, the relative L_2 error was plotted at each time step as shown in Figure 12. It can be observed that at very early time steps both approximations were inaccurate, but after approximately 0.1 seconds, the POD-GFEM produced significantly smaller errors than the FEM with the same mesh. The large errors in the first few time steps can be attributed to the sampling of the snapshots and the very localized nature of the solution. The accuracy of the approximation at early times can be improved by including additional snapshots sampled at these times. It is important to realize that even though the boundary conditions, material parameters, and heat source function considered in the problem at hand were also used for generating the snapshots, it was expected that four modes would not be sufficient to obtain an accurate approximation of the solution within the context of a conventional POD expansion. This was confirmed by computing the best approximation errors

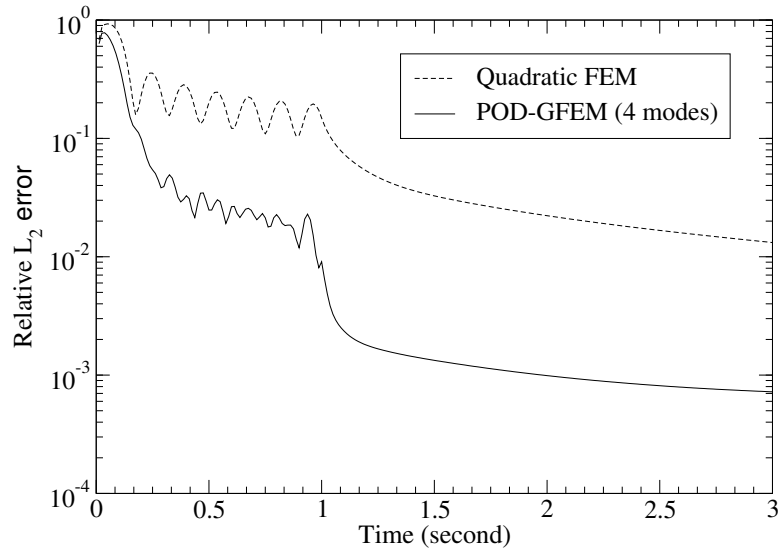


Figure 12. Relative L_2 error versus time.

for a conventional POD expansion using four modes, as well as for the corresponding basis in the POD-GFEM (see Eq. (18)). The average (in time) relative L_2 -errors for the POD expansion and for the POD-GFEM basis were 0.434 and 0.017, respectively. These numbers demonstrate the benefit of using POD modes in the context of GFEM over their use in conventional reduced order modeling.

5. CONCLUDING REMARKS

A methodology was presented that integrates proper orthogonal decomposition (POD) with the generalized finite element method (GFEM), which we referred to as POD-GFEM. It was shown through three examples that the approximation capabilities of POD modes can be effectively used in the GFEM. Best approximation studies revealed that using POD modes as enrichment

functions in the GFEM yields significantly better results than the individual POD modal expansions or FEM polynomial expansions. Furthermore, it was shown that very coarse meshes used in POD-GFEM yielded results as accurate as those of very fine finite element meshes. The smaller number of degrees of freedom needed for POD-GFEM, as compared to FEM, indicates that the method could be used for reduced order modeling with the added advantages that the modes and problem domains can be different, and that essential boundary conditions can be more easily handled than in conventional POD-based reduced order modeling.

Finally, we would like to point out that using energy or H_1 norms to determine the POD modes may be a more consistent approach in the context of the generalized finite element method. This effort is currently being undertaken by the authors.

6. ACKNOWLEDGMENTS

W. Aquino and J. C. Brigham would like to acknowledge the support provided by The National Institute of Biomedical Imaging and Engineering, Award No. EB2002167-17. In addition, C. J. Earls acknowledges the support of the Office of Naval Research, under Contract No. N00014-07-1-0515.

REFERENCES

1. Strouboulis T, Copps K, Babuška I. The generalized finite element method. *Computer Methods in Applied Mechanics and Engineering* 2001; **190**(32–33):4081–4193.
2. Melenk JM, Babuška I. The partition of unity finite element method: Basic theory and applications. *Computer Methods in Applied Mechanics and Engineering* 1996; **139**:289–314.
3. Babuška I, Melenk JM. Partition of unity method. *International Journal for Numerical Methods in Engineering* 1997; **40**:727–758.

4. Babuska I, Banerjee U, Osborn JE. On principles for the selection of shape functions for the Generalized Finite Element Method. *Computer Methods in Applied Mechanics and Engineering* 2002; **191**(49–50):5595–5629.
5. Belytschko T, Black T. Elastic crack growth in finite elements with minimal remeshing. *International Journal for Numerical Methods in Engineering* 1999; **45**(5):601–620.
6. Strouboulis T, Zhang L, Babuška I. Generalized finite element method using mesh-based handbooks: application to problems in domains with many voids. *Computer Methods in Applied Mechanics and Engineering* 2003; **192**(28–30):3109–3161.
7. Strouboulis T, Zhang L, Babuška I. p -version of the generalized FEM using mesh-based handbooks with applications to multiscale problems. *International Journal for Numerical Methods in Engineering* 2004; **60**(10):1639–1672.
8. Duarte CA, Kim DJ. Analysis and applications of a generalized finite element method with global-local enrichment functions. *Computer Methods in Applied Mechanics and Engineering* 2008; **197**(6–8):487–504.
9. Sukumar N, Pask JE. Classical and enriched finite element formulations for Bloch-periodic boundary conditions. *International Journal for Numerical Methods in Engineering* 2009; **77**(8):11211138.
10. Holmes P, Lumley J, Berkooz G. *Turbulence, Coherent Structures, Dynamical Systems, and Symmetry*. Cambridge University Press, 1996.
11. Aquino W. An object-oriented framework for reduced-order models using proper orthogonal decomposition (POD). *Computer Methods in Applied Mechanics and Engineering* 2007; **196**(41–44):4375–4390.
12. Stewart JR, Hughes TJR. A tutorial in elementary finite element error analysis: A systematic presentation of a priori and a posteriori error estimates. *Computer Methods in Applied Mechanics and Engineering* 1998; **158**:1–22.
13. Reddy BD. *Introductory Functional Analysis with Applications to Boundary-Value Problems and Finite Elements*. Springer, 1997.
14. Ravindran SS. A reduced-order approach for optimal control of fluids using proper orthogonal decomposition. *International Journal for Numerical Methods in Fluids* 2000; **34**(5):425–448.
15. Smith TR, Moehlis J, Holmes P. Low-dimensional modelling of turbulence using the proper orthogonal decomposition: A tutorial. *Nonlinear Dynamics* 2005; **41**(1-3):275–307.
16. Strouboulis T, Babuška I, Hidaajat R. The generalized finite element method for Helmholtz equation:

- Theory, computation, and open problems. *Computer Methods in Applied Mechanics and Engineering* 2006; **195**(37–40):4711–4731.
17. Langtangen H. *Computational Partial Differential Equations-Numerical Methods and Diffpack Programming*. 2nd edn., Springer, 2003.
 18. Jaynes ET. Information theory and statistical mechanics. *Physical Review* 1957; **106**(4):620–630.
 19. Ma X, Karniadakis GE, Park H, Gharib M. DPIV-driven flow simulation: a new computational paradigm. *Proceedings of the Royal Society of London Series a-Mathematical Physical and Engineering Sciences* 2003; **459**(2031):547–565.
 20. Ihlenburg F, Babuška I. Finite-element solution of the Helmholtz-equation with high wave-number 1. the h -version of the FEM. *Computers & Mathematics with Applications* 1995; **30**(9):9–37.
 21. Ihlenburg F. *Finite element analysis of acoustic scattering, Applied mathematical sciences*, vol. 132. Springer: New York, 1998.
 22. Aquino W, Brigham JC. Self-learning finite elements for inverse estimation of thermal constitutive models. *International Journal of Heat and Mass Transfer* 2006; **49**:2466–2478.